Fig. 4: Signal-to-noise ratios of angular galaxy clustering (D_g) in blue, ARF (D_z) in orange and the combinations $D_{g,z}$ in green and $D_{g,z,\kappa_{CMB}}$ in red. We used 20 tomographic Gaussian bins of $\sigma_z = 0.01$ in width in an *Euclid*-like survey, in combination with a CMB-S4 survey. The total signal-to-noise ratios for the range of multipoles $\ell = 10$ to $\ell = 300$ are shown in the text box on the bottom right.

probe-specific noise power spectra, and f_{sky} the sky fraction of the survey considered.

For the sake of simplicity, when combining galaxy surveys with CMB lensing, we always assume a full overlap of the two. As such, the sky fraction f_{sky} is always taken to be the one of either DESI or *Euclid*. Even if not accurate, this provides a rough estimate of the available constraining power that the combination of galaxy surveys with CMB lensing will be able to achieve.

We assumed that the noise of the angular galaxy clustering and that of the ARF were the shot noises arising from the discrete nature of galaxy surveys. We modelled it by replacing the power spectrum of dark matter by a Poissonian term, $P_{shot}(k,z) = 1/\bar{n}_g(z)$, in Eq. 12. From this, we can derive the following expressions for the shot noise:

$$N_\ell^{g_i,g_j} = \frac{\delta_{i,j}^K}{N_{gal}^i} , \qquad (24)$$

$$N_\ell^{z_i,z_j} = \frac{\delta_{i,j}^K}{\left(N_{gal}^i\right)^2} \int dV_\Omega \, \bar{n}_g(z) \, W(z_i,z) \, (z - \bar{z}_i)^2 , \qquad (25)$$

$$N_\ell^{g_i,z_j} = \frac{\delta_j^i}{\left(N_{gal}^i\right)^2} \int dV_\Omega \, \bar{n}_g(z) \, W(z_i,z) \, (z - \bar{z}_i) = 0 . \qquad (26)$$

We can see here that the shot noise cancels out when computing the cross-correlation between the angular galaxy density and the ARF fields.

The noise of the CMB lensing field reconstructed from *Planck* is taken from Planck Collaboration et al. (2020b). For the forecasted Simons Observatory CMB lensing noise, we took the publicly available noise curves provided by The Simons Observatory Collaboration et al. (2019).[1] In practice, we used the noise curves obtained with the internal linear combination (ILC)

component separation method, assuming the baseline analysis for a sky fraction of $f_{sky} = 0.4$. For CMB-S4, the lensing noise curve is taken as the minimum variance N0 bias, which is computed using the code `quicklens`.[2] We assume that CMB-S4 will have a beam size (full width at half maximum) of 1 arcmin, a temperature noise of $\Delta T = 1\,\mu K$ arcmin, and a polarisation noise of $\Delta P = \sqrt{2}\,\mu K$ arcmin (Abazajian et al. 2019).

For both the Simons Observatory and CMB-S4, $\ell = 40$ is the minimum multipole that will be accessible. We assume that these measurements will be combined with the *Planck* lensing signal for lower multipoles. As a result, we used the lensing noise of *Planck* for mutipoles below $\ell = 40$ when forecasting constraints with the Simons Observatory and CMB-S4.

We used the linear matter power spectrum $P(k)$ computed with the `CLASS` software (Blas et al. 2011). In order to focus on the linear regime we restrict our analysis to a maximum multipole of $\ell_{max} = 300$. Assuming the Limber approximation $k = (\ell + 1/2)/\chi(z)$, this ℓ_{max} corresponds to $k = 0.18\,h\,Mpc^{-1}$ at a redshift of $z = 0.65$. Given that we sample higher redshifts, we probe larger scales (k lower than $0.18\,h\,Mpc^{-1}$). We therefore expect little impact from non-linear physics in our observables (these are expected to become relevant on $k < 0.2\,h\,Mpc^{-1}$ at $z = 0$, and yet shorter at higher redshifts). Again, this is a conservative approach as one could consider a multipole cuttoff evolving with redshift as in Di Dio et al. (2014). We stress that, in our computations, we did not use the Limber approximation but the full computation of spherical Bessel functions.

Our minimum multipole was chosen to be $\ell_{min} = 10$. To reduce numerical noise and to speed up Fisher matrix computations, we performed a linear binning of the multipoles. In each multipole bin $[\ell_i, \ell_{i+1}[$, the binned C_ℓ is the average of the C_ℓ's that fall in the bin, and the binned multipole was taken as $\ell = (\ell_i + \ell_{i+1})/2$. We chose a bin size of $\Delta_\ell = 3$, which was applied to the full ℓ range. We checked that this binning did not impact the constraints from the Fisher matrix by comparing it with the case where we did not perform any multipole binning.

In Fig. 4, we show the signal-to-noise ratio for an *Euclid*-like survey combined with a CMB-S4 survey, for four probe combinations of: D_g, D_z, $D_{g,z}$, and $D_{g,z,\kappa_{CMB}}$ following the redshift binning shown in Fig. 1b. The total signal-to-noise for these four data vectors is, respectively, 544, 545, 778, and 786. This shows that the tomographic analysis of angular galaxy clustering and ARF have a similarly high signal-to-noise ratio. Moreover, the combined analysis $D_{g,z}$ brings more information than measuring the angular galaxy clustering alone D_g, as the signal-to-noise ratio is increased by 40%.

5. Fisher forecasts

We used the Fisher formalism to compute, a priori, how well our data vectors defined in Sect. 4 will constrain cosmological parameters in the context of future surveys. As we assumed that there is no correlation between different multipoles, the Fisher matrix can be summed over the multipoles and is given by

$$F_{i,j} = \sum_{\ell_{min}}^{\ell_{max}} \frac{\partial D(\ell)}{\partial \lambda_i} \, Cov_\ell^{-1} \, \frac{\partial D(\ell)}{\partial \lambda_j}, \qquad (27)$$

with D being one of the data vectors defined in Eqs. 19 to 20, $\{\lambda_i\}_i$ the set of free parameters of our model, and Cov_ℓ the covariance matrix given in Eq. 23.

Ω_b	Ω_m	n_s	h	σ_8	w_0	w_a
0.04897	0.3111	0.9665	0.6766	0.8102	-1	0

Table 2: Fiducial values of the free parameter of our fiducial cosmological model. We first consider only parameters in the standard ΛCDM model, and later we include the w_0, w_a parameters from the CPL parametrisation of dark energy.
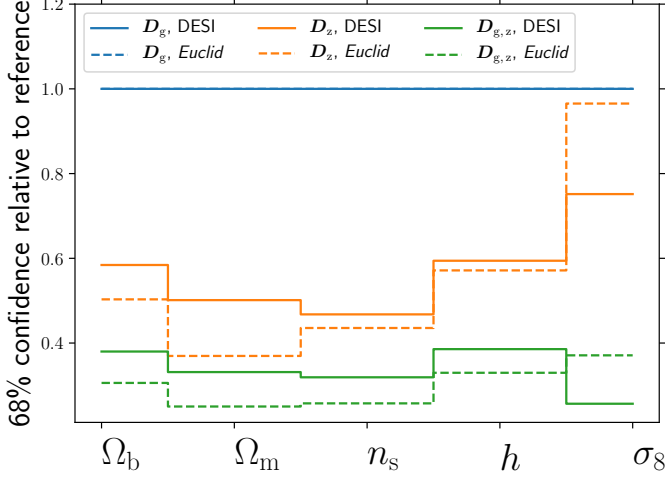

Fig. 5: Ratio of 1σ confidence interval relative to the 1σ value from angular galaxy clustering ($\boldsymbol{D}_g$) for ΛCDM parameters. Constraints are marginalised over the 20 galaxy bias parameters. Plain lines are for a DESI-like survey, while dashed lines are for an *Euclid*-like survey. Blue line shows $\boldsymbol{D}_g$ (our reference here), orange lines show $\boldsymbol{D}_z$, and green lines show $\boldsymbol{D}_{g,z}$. We see that for most parameters (except σ_8) confidence intervals shrink by $\sim 50\%$ when using $\boldsymbol{D}_z$ instead of $\boldsymbol{D}_g$. When using the combination $\boldsymbol{D}_{g,z}$, 1σ intervals are shrunk by at least 60% for all parameters.

The derivatives $\partial \boldsymbol{D}(\ell)/\partial \lambda_i$ are computed as the two-point variation with a 1% step around the fiducial value. We checked that our derivatives were numerically stable when changing the step size.

We computed forecasts for two cosmological models. The first one assumes the standard ΛCDM model, and the parameters we vary are $\left\{\Omega_m, \Omega_{baryon}, \sigma_8, n_s, h, \right\}$. The fiducial values of these parameters are given by Planck Collaboration et al. (2020a). The second model assumes an evolving dark energy equation of state, with the so-called CPL parametrisation (Chevallier & Polarski 2001; Linder 2003): $w(z) = w_0 + w_a z/(1 + z)$. Our second set of free parameters is then $\left\{\Omega_m, \Omega_{baryon}, \sigma_8, n_s, h, w_0, w_a\right\}$. In both cases, we assumed a flat universe ($\Omega_k = 0$) with massless neutrinos ($\sum m_\nu = 0$). In Tab. 2, we show the fiducial values of the free parameters.

We also considered a bias parameter assumed constant within each redshift bin, thus adding one free parameter for each redshift shell, over which we marginalised the Fisher analysis. The fiducial values of the galaxy bias depend on the survey considered and are given in Eqs. 1 and 2. We took the value at z_i, which is the centre of the Gaussian shell for each bin.
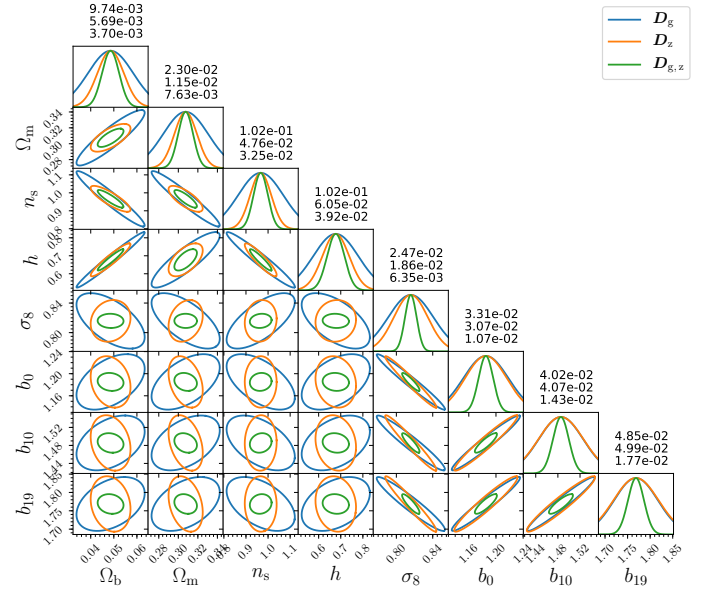

Fig. 6: Foreseen constraints (1σ contours) for a set of five ΛCDM parameters, plus three galaxy bias parameters (out of a total of 20) for a DESI-like survey. We assume 20 tomographic Gaussian bins of size $\sigma_z = 0.01$. The blue lines are the constraints for angular galaxy clustering alone $\boldsymbol{D}_g$, the orange lines are for the ARF alone $\boldsymbol{D}_z$, and the green line is a joint analysis of both fields $\boldsymbol{D}_{g,z}$. The figures above the 1-D PDFs give the marginalised 1σ uncertainty of the parameter for each data vector. We show here only three galaxy bias parameters, even if we marginalised upon the 20 bias parameters.
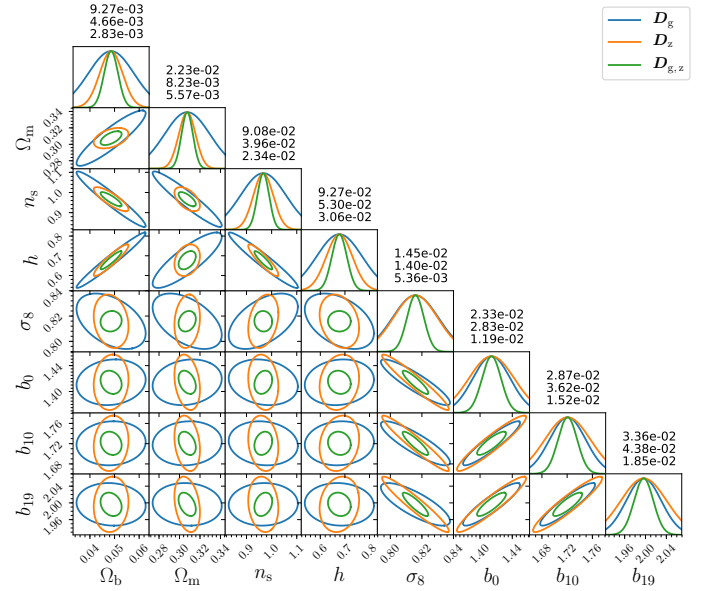

Fig. 7: Same as Fig. 6, but for an *Euclid*-like survey.

5.1. Results for the ΛCDM model

The results for the ΛCDM model are summarised in Fig. 5, where we show the ratio of the 1σ marginalised uncertainties when including ARF compared to using only angular galaxy clustering, for a DESI-like and a *Euclid*-like surveys. Figures 6

and 7 show the 1σ uncertainty ellipses for the ΛCDM parameters and three out of the 20 galaxy bias parameters for a DESI-like survey and an *Euclid*-like survey, respectively. Error ellipses for $\boldsymbol{D}_{\mathrm{g}}$, $\boldsymbol{D}_{\mathrm{z}}$, and $\boldsymbol{D}_{\mathrm{g,z}}$ are given by blue, orange, and green curves, respectively, while marginalised 1σ uncertainties for each parameter are quoted, for these three sets of observables, above the panels containing the 1D probability density distributions (PDFs).

For both types of LSS surveys, we can see in Fig. 5 that ARF ($\boldsymbol{D}_{\mathrm{z}}$) are significantly more sensitive than angular galaxy clustering ($\boldsymbol{D}_{\mathrm{g}}$), reducing the marginalised uncertainties of all cosmological parameters by a factor of two, except for σ_8, to which both observables are similarly sensitive. For the combined analysis $\boldsymbol{D}_{\mathrm{g,z}}$, marginalised uncertainties are reduced by more than 60 % for all parameters (including σ_8), compared to the angular galaxy clustering probe alone $\boldsymbol{D}_{\mathrm{g}}$. We find that using ARF in combination with angular galaxy clustering provides almost the same improvement on the constraints on cosmological parameters for both surveys, although the improvement is on average slightly better for our *Euclid*-like survey.

We see in Figs. 6 and 7 that while the degeneracy direction between different cosmological parameter pairs seems very similar for both angular galaxy clustering and ARF, this is again different for σ_8. For $\boldsymbol{D}_{\mathrm{z}}$, this parameter seems rather independent of other cosmological parameters, while its degeneracy with bias parameters is slightly tilted with respect to that of $\boldsymbol{D}_{\mathrm{g}}$. As a consequence, the joint $\boldsymbol{D}_{\mathrm{g,z}}$ ellipses show little degeneracy with other parameters, including bias. We also find that the marginalised constraints from both experiments are very close, although the *Euclid*-like experiment provides slightly more sensitive forecasts.

Figure A.1 in the appendix shows the correlation matrix between our free parameters (including galaxy bias parameters) and illustrates the opposite degeneracies that both $\sigma8$ and bias parameters have with the other parameters when comparing ARF and angular galaxy clustering.

Even for those parameters for which both angular galaxy clustering and ARF show a similar direction of degeneracy, the combination of the two observables yields significantly reduced error ellipses. This is mostly due to the lack of correlation between the ARF and angular galaxy clustering for narrow widths used in this work ($\sigma_{\mathrm{z}} \leq 0.01$), as noted in HMCMA and shown here in Fig. 3.

5.2. Extension to CPL dark energy parametrisation

We repeat the analysis detailed above including two new parameters describing the equation of state of dark energy following the CPL parametrisation: w_0 and w_a. In Fig. 8, we show the improvement on the marginalised uncertainties of the ARF with respect to angular galaxy clustering alone. We see that $\boldsymbol{D}_{\mathrm{z}}$ improves the constraints by 20 % to 50 % on this set of free wCDM parameters, for both surveys. The combined analysis $\boldsymbol{D}_{\mathrm{g,z}}$ reduces the uncertainties by at least 50 % and up to 80 % for Ω_{m}, σ_8, w_0 and w_a. The error ellipses are given in the appendix in Fig. B.1 for the DESI-like and *Euclid*-like experiments, displaying a pattern similar to what was found for ΛCDM, together with the correlation matrices (Fig. B.2).

In our idealised case, the combination of ARF with angular galaxy clustering greatly improves the sensitivity of these surveys to dark energy. As shown in Fig. 9, the figure of merit of w_0-w_{rma} increases by more than a factor of ten when ARF are combined with angular galaxy clustering. It increases from 17 to 189 for our DESI-like survey and from 19 to 345 for our *Euclid*-like survey.
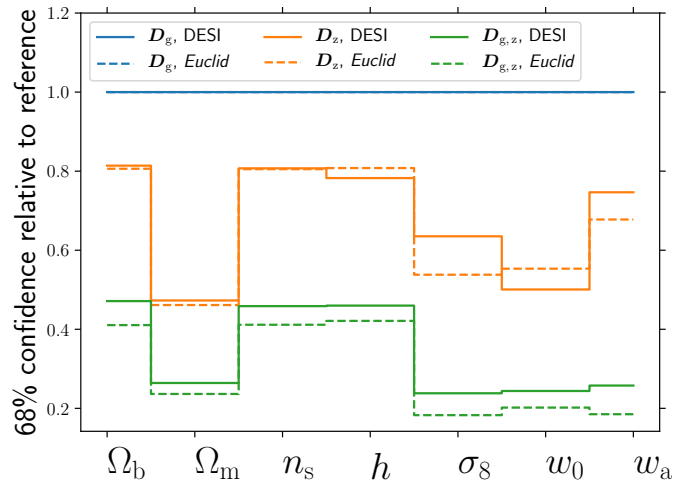

Fig. 8: Ratios of 1σ marginalised uncertainties relative to 1σ marginalised uncertainty for $\boldsymbol{D}_{\mathrm{g}}$. We assume a wCDM model and marginalise on 20 galaxy bias parameters (one for each redshift bin). Orange lines show the ratio for $\boldsymbol{D}_{\mathrm{z}}$ and green lines show the ratio for $\boldsymbol{D}_{\mathrm{g,z}}$. Solid lines are for a DESI-like survey, while dashed lines are for an *Euclid*-like survey. We see that $\boldsymbol{D}_{\mathrm{z}}$ improves constraints by up to 50 % compared to $\boldsymbol{D}_{\mathrm{g}}$, and the combined analysis $\boldsymbol{D}_{\mathrm{g,z}}$ improves constraints by up to 80 %.

5.3. Combining ARF and galaxy clustering with CMB lensing

In Figs 10 and 11, we show the improvements on the constraints of the ΛCDM and wCDM parameters for an *Euclid*-like survey, when combined with CMB lensing from *Planck*, the Simons Observatory, and CMB-S4, marginalised over the galaxy bias parameters. We see that including CMB lensing from *Planck* improves the constraints by maximum of 10 % in both cosmologies. The improvement is more significant when combining ARF and galaxy clustering with the Simons Observatory or CMB-S4. For the Simons Observatory and CMB-S4, in the ΛCDM model, marginalised uncertainties on Ω_{m} and σ_8 are decreased by up to 30 %. Other parameters are improved by 5 % to 10 %. For the wCDM model, the improvement is of $\sim$ 15 % for most parameters, with the most significant for Ω_{m} and w_a, with uncertainties decreased by up to 30 %. We see that the combination with CMB lensing helps to decrease uncertainties on the wCDM cosmology.

Since the CMB lensing is an unbiased probe of the distribution of matter, one of the main interests of combining it with galaxy surveys is to produce tight constraints on the galaxy bias parameter. In Fig. 12, we show the 1σ marginalised uncertainties on the galaxy bias parameters for each of the 20 redshift bins in an *Euclid*-like survey combined with CMB-S4 lensing, for the ΛCDM model. We compared the constraints obtained for angular galaxy clustering alone ($\boldsymbol{D}_{\mathrm{g}}$), with the ones obtained when combined with CMB lensing ($\boldsymbol{D}_{\mathrm{g},\kappa_{\mathrm{CMB}}}$), with ARF ($\boldsymbol{D}_{\mathrm{g,z}}$), and then the full combination ($\boldsymbol{D}_{\mathrm{g,z},\kappa_{\mathrm{CMB}}}$).

We see that the combination of angular galaxy clustering with ARF provides better constraints on the galaxy bias than the combination with CMB lensing. For instance, at a redshift of 1.06, the marginalised uncertainties for the galaxy bias parameter b_3 is of 0.025 for the angular galaxy clustering, it decreases to 0.020 when combined with CMB lensing, and down to 0.013 when combined with ARF. The combination of the three results in marginalised uncertainties of 0.08. We can see that the CMB
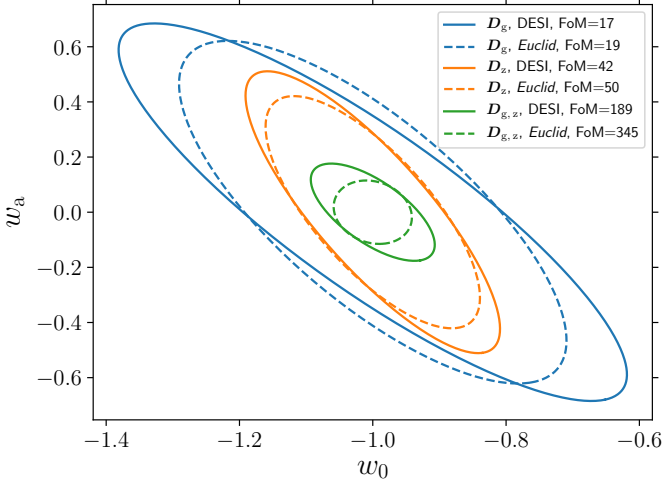
Fig. 9: Marginalised constraints (1σ contours) on the dark energy equation of state parameters for the DESI-like (solid lines) and for the *Euclid*-like (dashed lines) surveys, assuming 20 tomographic Gaussian bins of $\sigma_z = 0.01$. The blue lines are the constraints for angular galaxy clustering alone, the orange lines are for ARF alone, and the green lines are a joint analysis of both fields, $\boldsymbol{D}_{g,z}$. These contours are marginalised over the set of cosmological parameters as before, and over the galaxy bias in the 20 redshift bins. We display the figure of merit (FoM) of this pair of parameters in the upper right box for each combination of observables and for each survey.
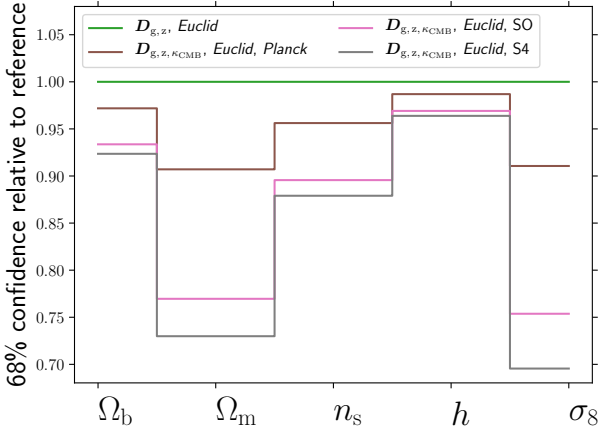
Fig. 10: Ratio of 1σ constraints for ΛCDM parameters from $\boldsymbol{D}_{g,z,\kappa_{CMB}}$ over the 1σ constraints from $\boldsymbol{D}_{g,z}$ for the *Euclid*-like spectroscopic survey. We show combinations with CMB lensing from *Planck* (brown), the Simons Observatory (pink), and CMB-S4 (grey). Constraints are marginalised over the 20 galaxy bias parameters.

lensing improves constraints by $\sim 20\,\%$ only, while ARF improves constraints by $\sim 50\,\%$ (a factor of two improvement). We argue that this is due to the importance of the velocity term in the ARF kernel (see Fig. 2), which does not depend on galaxy bias as it is sensitive to the full matter distribution.
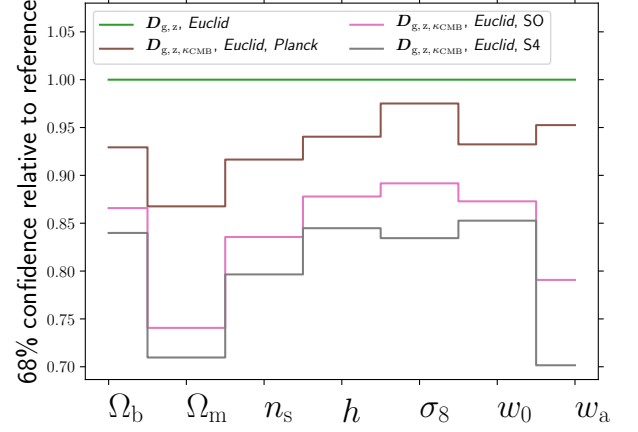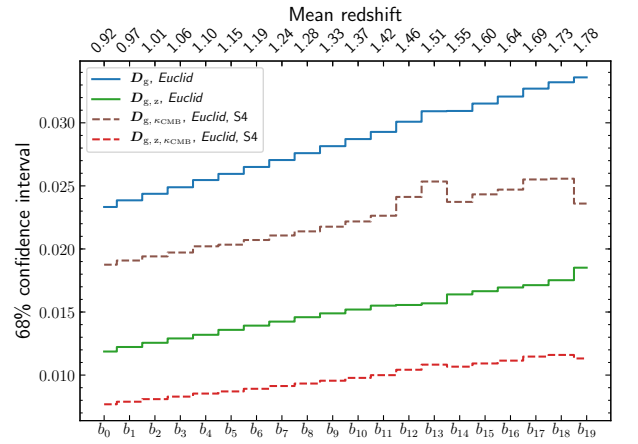
Fig. 11: Same as Fig. 10 for wCDM parameters.

Fig. 12: Marginalised 1σ confidence values for galaxy bias parameters, with an *Euclid*-like survey alone (plain lines) or in combination with the CMB-S4 lensing survey (dashed lines). We marginalised the five free parameters of the ΛCDM model. We show constraints with angular galaxy clustering (blue and brown lines) and in combination with ARF (green and red lines). The mean redshift of each shell is shown at the top. We see that the ARF combined with angular galaxy clustering $\boldsymbol{D}_{g,z}$ provides better constraints on galaxy bias than the combination of angular galaxy clustering with CMB lensing $\boldsymbol{D}_{g,\kappa_{CMB}}$.

6. Discussion

One could argue several reasons why angular observables might be preferred over standard 3D ones. Probably the main one is the lack of assumption of any fiducial cosmological model to analyse the data. This means that angular observables may be directly compared with theoretical predictions without any intermediate data manipulations that hinge on an assumption of which the implications in the analysis may not always be clear. Moreover, this type of angular analysis is conducted tomographically in moderately narrow redshift shells, thus avoiding the assumption that the universe remains effectively frozen in relatively long time spans, as it may occur in 3D clustering analysis where an effective redshift must be defined for the entire volume under analysis (see, e.g. Cuesta et al. 2016). Asorey et al. (2012) and Di Dio et al. (2014) have shown that when using a

large number of narrow redshift slices, a 2D clustering analysis can produce the same constraints on cosmological parameters as a 3D clustering analysis, provided that the width of the redshift slices is comparable to the minimum scale probed in the 3D analysis. By including the redshift information in a 2D field, the ARF observable keeps some information about the distribution of galaxies along the line of sight, which normally disappears when projecting the 3D galaxy density field on a 2D observable. As we have shown, ARF improve the usual 2D galaxy clustering analysis.

Another major interest of using angular observables is that they can easily be cross-correlated with other 2D observables. Indeed, the combination of 3D probes with 2D probes is not straightforward, especially when one has to properly take into account the covariances between them (see e.g. Passaglia et al. 2017; Camera et al. 2018). In this work, we used the CMB lensing field and its cross-correlation with our tomographic analysis of angular galaxy clustering and ARF. We have shown that these cross-correlations improve the constraints, especially on the galaxy bias. Chaves-Montero et al. (2019) showed that the cross-correlation of the ARF field with the CMB temperature field can detect the kinematic Sunyaev-Zel'dovich (kSZ) effect at the 10σ level.

The point of this paper is not a detailed comparison between 2D and 3D clustering analyses, but rather an exploration of the added value of including ARF in cosmological studies of the large-scale structures, on top of the traditional angular galaxy clustering. By their intrinsically different sensitivity to the cosmic density and velocity fields under the redshift shells, the ARF change the degeneracies between cosmological parameters, especially with respect to σ_8 and the galaxy bias, compared to the angular galaxy clustering. This is due, as claimed in HMCMA, to the fact that angular galaxy clustering is sensitive to the first moment (the average) of matter density and velocity under the redshift shells, whereas ARF are sensitive to the variation of matter density and velocity along the line of sight inside these redshift shells. Moreover, we have shown that the ARF and the angular galaxy clustering inside the same tomographic redshift bin are almost uncorrelated. Due to this absence of correlation, by combining both we are able to break degeneracies and give tighter constraints on all the cosmological parameters we considered.

The results we obtained in our work can be considered as an optimistic setting for both galaxy and CMB surveys. We restricted our analysis to the linear regime and we did not include any systematic effects that could impact our results and worsen the constraints. Hernández-Monteagudo et al. (2020) found that the impact of non-linear physics is more severe in angular galaxy clustering than in ARF. They found that a linear bias was sufficient to describe the ARF on scales larger than 60 h^{-1} Mpc, while it was not the case for angular galaxy clustering. Indeed, ARF are built upon the average observed redshift along the line of sight in a redshift selection function. This is intrinsically different to counting the number of galaxies in a given region in the universe, and consequently systematics and non-linearities affect each observable differently. In future works, we plan to address systematics and non-linearities, aiming to model more realistic settings. We expect that the impact of both systematics and non-linearities will depend on the survey and on the targeted galaxy sample, as ongoing work on existing galaxy surveys indicates.

We do not provide a detailed comparison with the forecasted constraints of the *Euclid* survey published in Euclid Collaboration et al. (2020). Indeed, our analysis considers a simplistic, linear model of the galaxy clustering. In this context, our findings indicate that ARF brings significant cosmological in-

formation on top of the traditional angular galaxy clustering. At best, our results with the angular galaxy clustering probe ($\boldsymbol{D}_g$) could be compared with the linear setting shown in Table 9 of Euclid Collaboration et al. (2020, first line). In that case, their probe is the 3D linear galaxy power spectrum, with a cutoff value at $k_{max} = 0.25$ h Mpc^{-1}, in four different redshift bins. Their Fisher analysis accounts for more parameters describing the anisotropies in the power spectrum and the shot noise residuals. This 3D probe is intrinsically different to the (2D) angular power spectrum tomography used in our work, in 20 Gaussian bins, which we limit to $k_{max} = 0.20$ h Mpc^{-1}. Our forecasts with $\boldsymbol{D}_g$ for the errors on some parameters are tighter than theirs (by a factor of ~ 2 for σ_8), while for others we find the opposite situation (e.g. the reduced Hubble parameter h, whose uncertainty in Euclid Collaboration et al. 2020 is roughly one third of ours).

7. Conclusion

We show that the ARF are a promising cosmological observable for next generation spectroscopic surveys. We find that for our choice of binning the tomographic analysis of ARF retrieves more information than the tomographic analysis of the angular galaxy clustering. We show that the joint analysis of both fields helps in breaking degeneracies between cosmological parameters, due to their lack of correlation and their different sensitivities to cosmology. The improvement appears to be particularly significant for the wCDM model. We show that the figure of merit for the w_0-w_a parameters was increased by a factor of more than ten when combining angular galaxy clustering with ARF.

Finally, we have seen that combining angular galaxy clustering with ARF provides tighter constraints on the galaxy bias parameters compared to the combination of angular galaxy clustering with CMB lensing. This shows that ARF are a very powerful probe of the distribution of matter, as they make it possible to break the degeneracy between σ_8 and the galaxy bias. For future galaxy surveys, errors on the cosmological figure of merit will be dominated by systematic uncertainties and non-linearities, and ARF might provide a novel and complementary view on those issues.

In our analysis, we did not consider massive neutrinos. As the growth rate is particularly sensitive to them, we expect ARF to be a powerful tool to constrain the mass of neutrinos. We defer this detailed analysis to an upcoming work.

Simultaneously, from the LSS and CMB fronts, the coincidence in the acquisition of excellent-quality, extremely large data sets should enable the combination of standard analyses with new, alternative ones, like the one introduced in this paper. The combination of techniques and observables should work jointly on the efforts of identifying and mitigating systematics, and pushing our knowledge of cosmological physics to its limits.

References

Abazajian, K., Addison, G., Adshead, P., et al. 2019, arXiv e-prints, arXiv:1907.04473
Abbott, T. M. C., Abdalla, F. B., Alarcon, A., et al. 2018, Phys. Rev. D, 98, 043526

Asorey, J., Crocce, M., Gaztañaga, E., & Lewis, A. 2012, MNRAS, 427, 1891

Benitez, N., Dupke, R., Moles, M., et al. 2014, arXiv e-prints, arXiv:1403.5237

Blas, D., Lesgourgues, J., & Tram, T. 2011, J. Cosmology Astropart. Phys., 2011, 034

Bonifacio, P., Dalton, G., Trager, S., et al. 2016, in SF2A-2016: Proceedings of the Annual meeting of the French Society of Astronomy and Astrophysics, ed. C. Reylé, J. Richard, L. Cambrésy, M. Deleuil, E. Pécontal, L. Tresse, & I. Vauglin, 267–270

Camera, S., Fonseca, J., Maartens, R., & Santos, M. G. 2018, MNRAS, 481, 1251

Cenarro, A. J., Moles, M., Cristóbal-Hornillos, D., et al. 2019, A&A, 622, A176

Chaves-Montero, J., Hernández-Monteagudo, C., Angulo, R. E., & Emberson, J. D. 2019, arXiv e-prints, arXiv:1911.10690

Chevallier, M. & Polarski, D. 2001, International Journal of Modern Physics D, 10, 213

Cuesta, A. J., Vargas-Magaña, M., Beutler, F., et al. 2016, MNRAS, 457, 1770

de Jong, R. S. & 4MOST Consortium. 2015, in IAU General Assembly, Vol. 29, 2255843

DESI Collaboration, Aghamousa, A., Aguilar, J., et al. 2016, arXiv e-prints, arXiv:1611.00036

Di Dio, E., Montanari, F., Durrer, R., & Lesgourgues, J. 2014, J. Cosmology Astropart. Phys., 2014, 042

Doré, O., Bock, J., Ashby, M., et al. 2014, arXiv e-prints, arXiv:1412.4872

Euclid Collaboration, Blanchard, A., Camera, S., et al. 2020, A&A, 642, A191

Hernández-Monteagudo, C., Chaves-Montero, J., & Angulo, R. E. 2019, arXiv e-prints, arXiv:1911.12056

Hernández-Monteagudo, C., Chaves-Montero, J., Angulo, R. E., & Ariccò, G. 2020, arXiv e-prints, arXiv:2005.06568

Hu, W. & Jain, B. 2004, Phys. Rev. D, 70, 043009

Hu, W. & Okamoto, T. 2002, ApJ, 574, 566

Huterer, D., Knox, L., & Nichol, R. C. 2001, ApJ, 555, 547

Ivezić, Ž., Kahn, S. M., Tyson, J. A., et al. 2019, ApJ, 873, 111

Krause, E. & Eifler, T. 2017, MNRAS, 470, 2100

Lacasa, F. 2018, A&A, 615, A1

Lahav, O., Lilje, P. B., Primack, J. R., & Rees, M. J. 1991, MNRAS, 251, 128

Laureijs, R., Amiaux, J., Arduini, S., et al. 2011, arXiv e-prints, arXiv:1110.3193

Lewis, A. & Challinor, A. 2006, Phys. Rep., 429, 1

Linder, E. V. 2003, Phys. Rev. Lett., 90, 091301

Linder, E. V. 2005, Phys. Rev. D, 72, 043529

Martí, P., Miquel, R., Castander, F. J., et al. 2014, MNRAS, 442, 92

Moles, M., Benítez, N., Aguerri, J. A. L., et al. 2008, AJ, 136, 1325

Newman, J. A., Cooper, M. C., Davis, M., et al. 2013, ApJS, 208, 5

Okamoto, T. & Hu, W. 2003, Phys. Rev. D, 67, 083002

Omori, Y., Chown, R., Simard, G., et al. 2017, ApJ, 849, 124

Padmanabhan, N., Schlegel, D. J., Seljak, U., et al. 2007, MNRAS, 378, 852

Passaglia, S., Manzotti, A., & Dodelson, S. 2017, Phys. Rev. D, 95, 123508

Pérez-González, P. G., Cava, A., Barro, G., et al. 2013, ApJ, 762, 46

Planck Collaboration, Aghanim, N., Akrami, Y., et al. 2020a, A&A, 641, A6

Planck Collaboration, Aghanim, N., Akrami, Y., et al. 2020b, A&A, 641, A8

Pozzetti, L., Hirata, C. M., Geach, J. E., et al. 2016, A&A, 590, A3

Scoville, N., Aussel, H., Benson, A., et al. 2007, ApJS, 172, 150

Sherwin, B. D., van Engelen, A., Sehgal, N., et al. 2017, Phys. Rev. D, 95, 123529

The Simons Observatory Collaboration, Ade, P., Aguirre, J., et al. 2019, J. Cosmology Astropart. Phys., 2, 056

Wu, W. L. K., Mocanu, L. M., Ade, P. A. R., et al. 2019, ApJ, 884, 70

Appendix A: Correlation matrices

The correlation matrices in Fig. A.1 provide an alternative view of our results. It shows the correlation matrices for the five ΛCDM parameters and the 20 galaxy bias parameters for a DESI-like survey. We see the opposite correlation of the cosmological parameters Ω_b, Ω_m, n_s, and h with σ_8 for angular galaxy clustering and ARF. This opposite correlation is mirrored in the correlations of those three cosmological parameters with galaxy bias parameters. This is expected, as σ_8 and bias are tightly correlated. The different nature of the correlation of σ_8 and bias with the other cosmological parameters for angular galaxy clustering and ARF is critical for (partially) breaking degeneracies when combining angular galaxy clustering with ARF.

Appendix B: Results for the wCDM model

We show the ellipses obtained with our Fisher analysis for the wCDM model in Fig. B.1, for a DESI-like and an *Euclid*-like survey. For many parameter pairs, the degeneracy direction (or ellipse orientation) for angular galaxy clustering and ARF are similar, although the resulting error ellipse in the joint $D_{g,z}$ probe shrink very significantly in all cases. As a result, foreseen uncertainties in the parameters are divided by a factor of at least two for all parameters.

In Fig. B.2, we show the correlation matrices for the wCDM model. It turns out that for D_z the new parameters, w_0, w_a, together with σ_8, constitute an almost separate (or largely un-correlated) box with respect to all other parameters (see Fig. B.2b). This does not seem to be the situation for angular galaxy clustering D_g (Fig. B.2a), although this characteristic remains (to a great extent) for the joint observable set ($D_{g,z}$, Fig. B.2c).
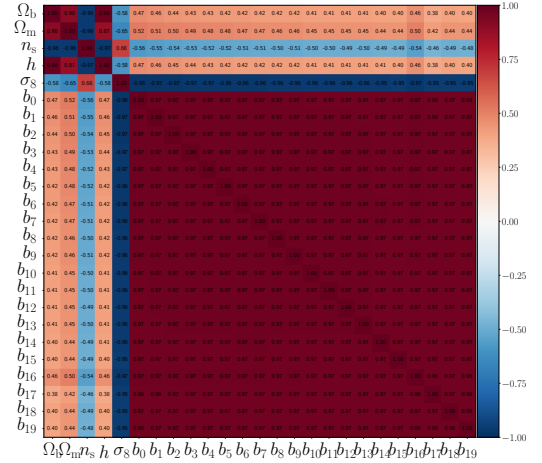
(a) D_g
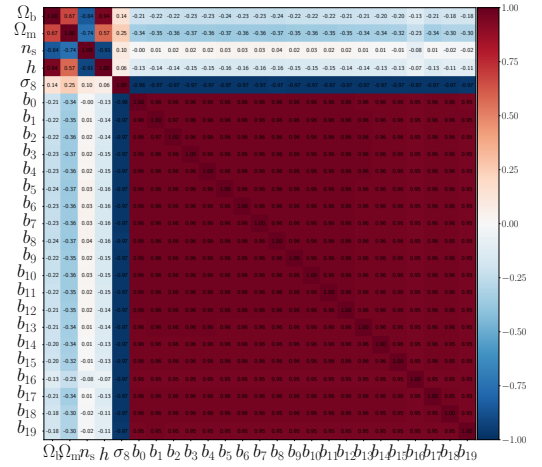
(b) D_z
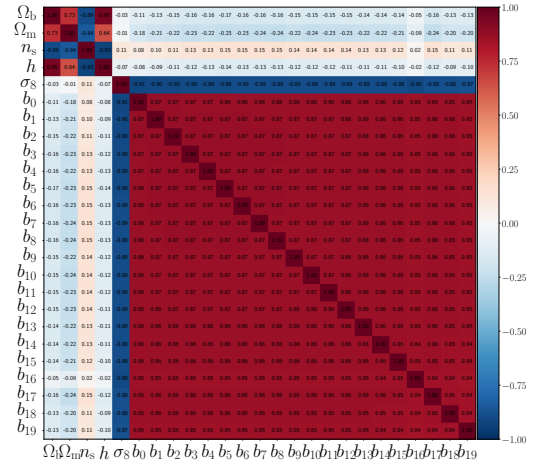
(c) $D_{g,z}$

Fig. A.1: Correlation between parameters of the ΛCDM model for a DESI like survey. The top panel is for the angular galaxy clustering alone, the central panel is for ARF alone, and the bottom panel is for a combination of both observables. We see that the angular galaxy clustering and ARF have opposite correlation coefficients between cosmological parameters and the galaxy bias. The combination of both helps significantly to break degeneracies with the galaxy bias.
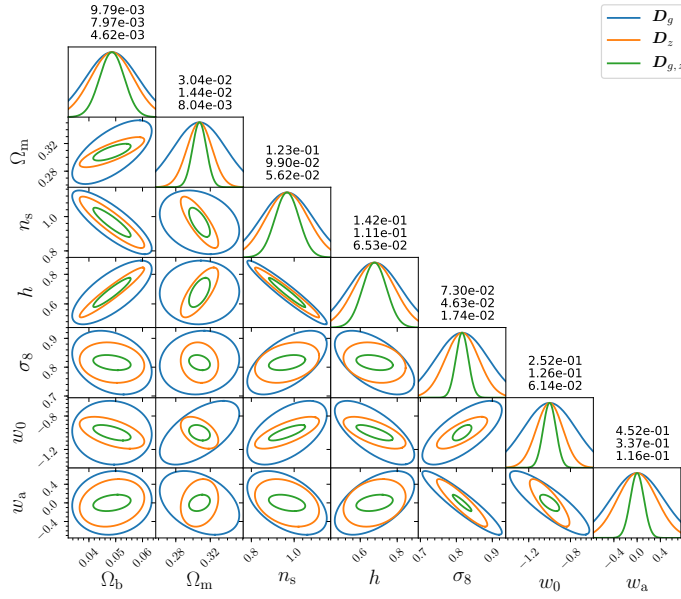
(a) DESI
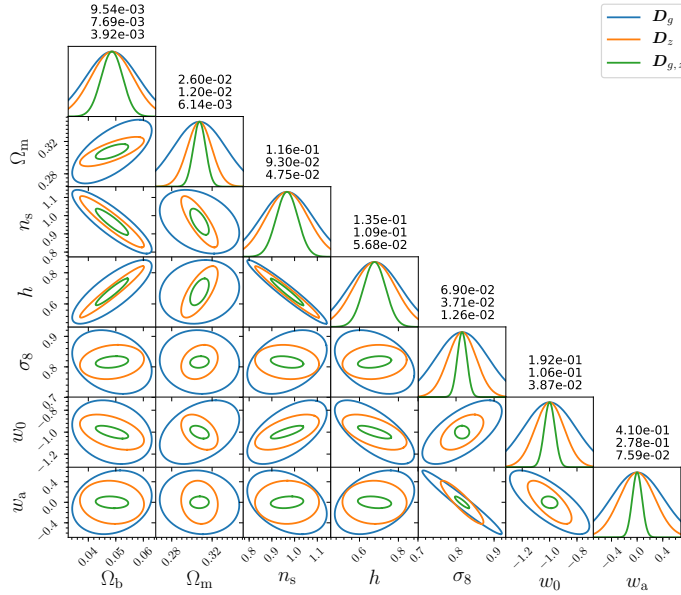
(b) *Euclid*

Fig. B.1: Foreseen constraints (1σ contours) in CPL cosmological extension wCDM for a DESI-like survey (top) and an *Euclid*-like survey (bottom), assuming 20 tomographic Gaussian bins of $\sigma_z = 0.01$. The blue lines are the constraints for angular galaxy clustering alone (D_g), the orange lines are for the ARF alone (D_z), and the green line is a joint analysis of both fields ($D_{g,z}$). These contours are marginalised over the galaxy bias in the 20 redshift bins. The numbers above the parameter PDFs give the marginalised 1σ uncertainty of each parameter for each data vector.
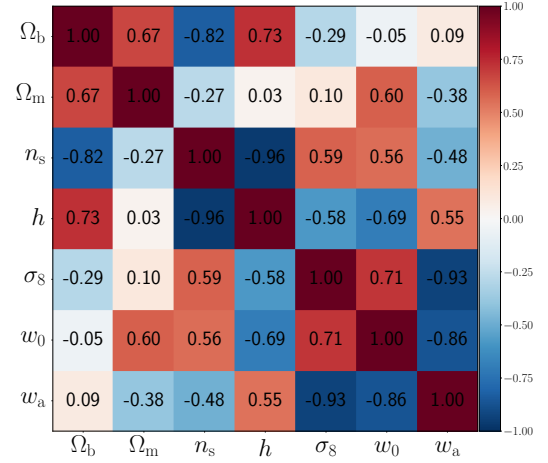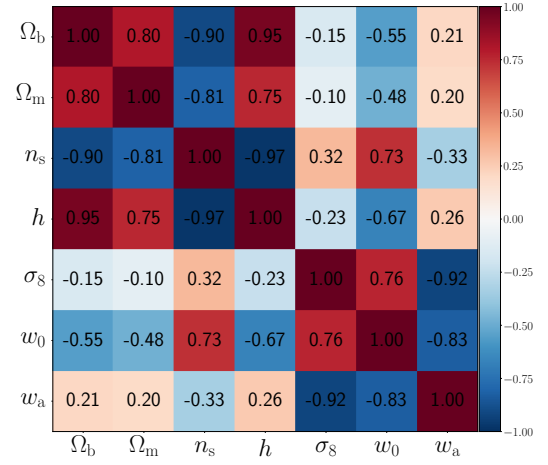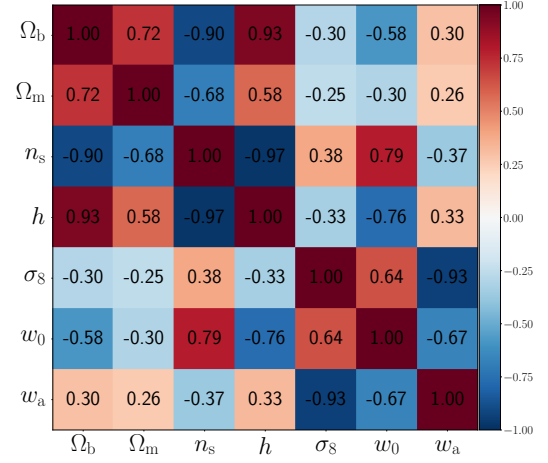

(a) D_g

(b) D_z

(c) $D_{g,z}$

Fig. B.2: Correlation between parameters of the wCDM model, marginalised over the galaxy bias for a DESI-like survey. The top panel is for the angular galaxy clustering (D_g), the central panel refers to ARF alone (D_z), and the bottom panel is for a combination of both observables ($D_{g,z}$). We find that D_z show different correlations compared to D_g. The combination of both helps significantly to break degeneracies, as we can see in panel (c).